Multi-objective design optimization of a frontal crash energy absorption system for a road-safe vehicle

Tiago Nunes
tiagomenunes@tecnico.ulisboa.pt

Instituto Superior Técnico, Universidade de Lisboa, Portugal

November 2017

Abstract

Since 2013, more than 1.25 million people die each year in road accidents, making road safety a global concern. With regard to protection in frontal and rear collisions, a common solution is to use a structure designed to deform in a controlled manner in the event of collision, avoiding deformation of the cabin and excessive accelerations in the passengers, which can lead to serious injuries or even fatalities. This work focus on the development of an aluminum structure of this type, aiming for an optimized design, within the design parameters available for the vehicle project in which it is included. A Finite Element Analysis (FEA) model of the frontal energy absorption structure for frontal impact is developed and validated with a quasi-static compression experimental procedure. A multi-objective optimization process, that can be adaptable to the future needs of the project, is developed. Several changes in the geometry are tested, focusing on specific deficits in the performance of the structure. Through this process, a robust and adaptable FEA model is achieved and a compilation of the influence of several parameters on the impact performance is obtained. The optimized structure shows a significant performance improvement in the event of a frontal collision and, according to the established limits, it is expected to satisfy the legal values of safety in the tests carried out by the responsible entities.
Keywords: thin-walled beams, front collision, energy absorption, crash performance, multi-objective optimization

1. Introduction

Since the introduction of automobile structures mass production by Henry Ford in 1913, a continuous technological development in road vehicles performance took place. The majority of the consequences for the world society have been positive but, with the increasing in the number of vehicle and travel speeds, the fatalities caused by crashes have become a major concern [1]. According to the World Health Organization (WHO), by the year 2030, road accidents will reach fifth place among the leading death causes in the world, making the development of automotive safety systems a vital subject for research.

In order to improve the safety of roads worldwide, numerous works have been made aiming for a decrease in vehicle crashes and an improvement of the ability of the vehicle to protect the occupants from injury. With the development of safety systems in automotive industry, the number of deaths between 2005 and 2014 in the EU have decreased from 46,000 to 26,000.

The ability of the vehicle to absorb energy and to prevent occupant injuries in the event of an accident is referred to as "Crashworthiness". This ability can be improved by developing more efficient Energy Absorption (EA) systems, that have been studied by many authors due to their relevance.

In the case of frontal crash, the main automotive part which undergoes impact stress is the bumper. This makes the study of bumper's design and manufacturing a relevant and crucial subject. Bumpers are solid structures that should be stiff enough to maintain the integrity of the car and have sufficient ductility to suffer plastic deformation, in the case of metals, to absorb the kinetic energy transmitted during the collision process. In most cases, bumpers are simple structures, composed by one or more beams connected to the vehicle's chassis.

On impact, this structural part of a vehicle has two main functions. Absorb kinetic energy of the vehicle while keeping an allowable deceleration for the survival of occupants and preserve the integrity of the passenger compartment and so avoid the intrusion of rigid components into it.

When talking about automotive crash, there are several entities responsible to access the crash performance of road vehicles. The standard tests are

made by United Nations Economic Commission for Europe (ECE) and National Highway Traffic Safety Administration (NHTSA) in the USA. In these tests, the setup is defined by standard regulations and the results are compared to maximum values of accelerations and forces suffered by the dummies during the crash. NHTSA issues Federal Motor Vehicle Safety Standards (FMVSS) to implement laws from Congress. These regulations allow to fulfill their mission to prevent and reduce vehicle crashes. The main requirements to be within the safety limits are defined to the vital body parts, in particular chest and head by three criteria. The Head Injury Criterion (HIC) defined by

$$HIC = \left[\frac{1}{t_2 - t_1}\int_{t_1}^{t_2} a dt\right]^{2.5}(t_2 - t_1), \qquad (1)$$

is limited by a maximum allowable value of 1000, being a the resultant acceleration expressed as a multiple of g, and $t1$ and $t2$ are any two points in time during the crash of the vehicle which are within a 15 ms time interval. The chest must not suffer a compression superior to 76.2 mm and an acceleration higher than 60 G's. These standards are defined by FMVSS [2] for an impact in a fixed barrier either perpendicular or at a 30^o angle at a speed of 30 mph ($\simeq$ 48 km/h) for the front-seated Hybrid III dummy occupants. Some independent associations started to test a great number of vehicles available in the market and developed scoring systems. The most relevant entity performing these tests is1 New Car Assessment Programme (NCAP). NCAP's frontal impact tests consist in a frontal impact test into a fixed barrier at 50 km/h and a 40% overlap impact onto a deformable barrier at 64 km/h.

This work was included in Be2 project at CEiiA. The project goal is to to create Be2, a M1 class electric powered and road safe vehicle that can be implemented in the sharing platform mobi.me, a fully integrated and user-centric management of mobility devices. During this work, a robust numerical model for a complete front bumper structure is created and used to evaluate different solutions. Using suitable criteria, a multi-objective optimization procedure is used to access the quality of the structures and understand the influence of a set of parameters in the crash performance of the structure. The model is then validated using the available experimental procedures. An optimized solution that is expected to perform well in the tests specified by the responsible entities regarding front collision of vehicles is obtained.

2. Approach

In this work, a conventional bumper composed by a transverse beam and two crash boxes was modeled and sized. They are expected to be deformable enough to absorb the impact energy to reduce the risk of injury for pedestrians and other vulnerable road users but, at the same time, should also have sufficient strength and stiffness to give place to small intrusion of the engine compartment and, therefore, to protect the nearby vehicle components.

In the beginning of the design phase it is important to study the benefits of the available materials and choose a suitable one for the structure. The structural study of a component or a full vehicle can be approached in a wide variety of methodologies and models. To have a good understanding of the structure behaviour in the studied situation, the choice of the simulation is critical to obtain meaningful results and conclusions about the expected behaviour of the structure in a specific test and save computation time translating into cost savings. Essentially, the expected behaviour of the structure has to be studied before the computational model is developed.

2.1. Material Model

For automotive structural purposes, the most used alloys are the ones of the 6000 and 7000 series because they have high stiffness and are heat treatable . The 6061 magnesium and silicone alloy is the best choice whenever welding or brazing is required. The heat treatment makes possible a change in the mechanical properties of the metal to fulfill to the demands of the design. In the present work, a 6061 T6 alloy was used, because it is more suitable for energy absorption structures due to its maximizing strength [3].

To get the best correlation with the experimental data, it is important to chose the appropriate theoretical model to simulate the properties of the material being tested. The most common way for taking account plasticity is to set a tabulated function that gives the link between stresses and plastic strains. The problem with this approximation is that it does not consider the changing in properties of the materials with different conditions. A solution is to use a model that has been used in similar studies and proven to work for similar cases with the best proximity to the real impact test. In impact analysis, the material constitutive law should include strain rate dependency for both material deformation and failure.

G. R. Johnson and W. Cook made several studies [4] and developed a model that respect this requirement. This model was used and validated by some authors for low and high velocity impact situations. Some papers focus in the study of strain-rate forms implemented in modified Johnson-Cook constitutive model and conclude that the standard model strain-rate form provides the best overall compar-

ison with the data [5]. Considering these results, it is expected that this model fits the crash tests intended by the present study and have good correlation with the experimental results.

Using Johnson-Cook formulation, the material stress strain curve is built in two parts. Before the start of the plastic deformation, the stress-strain curve is linear, respecting 3D Hook's Law. When the stress reaches the yield strength value of the material, the plastic strain starts. After this point, the curve is defined by the Johnson-Cook Flow Surface[6],

$$\sigma = [A + B(\bar{\varepsilon}^p)^n]\,[1 + Cln(\dot{\varepsilon}^*)][1 + (T^*)^m], \quad (2)$$

where A, B, C, n and m are constants, σ is the stress value in the plastic regime, T^* is the non-dimensional temperature, $\dot{\varepsilon}^*$ is the non-dimensional strain rate and $\dot{\bar{\varepsilon}}^p$ is the effective plastic strain rate.

In several studies, the influence of strain rate was studied and, as described by A. Manes et al [7], for strain rates lower than 1000 s^{-1}, this influence is not significant. Higher values of strain rates are observed mostly on ballistic tests and is not expected that, in a crash situation, the material suffers a strain rate higher than that value. Also the temperature dependence is negligible in this case because the value of T^* will be small while the temperature of the specimen is close to room temperature and the room temperature is considerably lower than the melting temperature. If the change in temperature and the strain rate are not considered, the model gets simplified by

$$\sigma = [A + B(\bar{\varepsilon}^p)^n]\,. \quad (3)$$

2.2. Dynamic Explicit Analysis

In crash tests, the problem should be treated as fully dynamic because the velocity and inertia of the vehicle takes a big role in the behaviour of the whole structure. Knowing this, it is important to evaluate if the behaviour of the structure is expected to be linear or have non-linearities. Both static and dynamic problems can be treated as linear or non-linear.

Linear behaviour in structural problems means that the structure stress never surpasses the yield limit and it should only be used in small deflection problems, usually the criterion is that the deflection should not be larger than half of the structure thickness. Thus assuming a linear relation between stress and strain contacts usually have a non-linear behaviour, so using contacts in linear static analysis is also a bad approach. Non-linear analysis allows the introduction of non-linearities in the problem that can be associated to materials, geometries or contacts. In studies with high plastic deformation or even when rupture is expected, for example crash tests, the material model is highly non-linear.

In terms of computation, non-linear problems are usually solved with Implicit or Explicit solvers. A choice must be made taking into account that none of this type of solver is better for every problem. Both solvers can introduce and compute non-linearities but both have limitations. In Table 1 there are some criteria that can help chosing between implicit and explicit numerical softwares.

Table 1: Explicit and implicit choice criteria

Implicit Non-Linear	**Explicit Non-Linear**
Long Event (Few Seconds)	Short Events (ms)
Small deformation	Large deformation
Low number of contacts	High number of contacts
Simple material models	Wide variety of material options

In a car crash, the total time of the impact can have less than 100 milliseconds, the deformation of the frontal impact absorption system should be large enough to absorb the kinetic energy and protect the cabin and the components suffer high deformations, sometimes even fractures. Taking the previous criteria into account, the obvious choice is to use an explicit software so that the computational model can have better resemblance to a real crash. Explicit analysis is the best option for dynamic highly non-linear problems.

3. Numerical Model

Due to the unfeasibility of dynamic crash experimental tests, the best option with the available means to validate the model is to perform a quasi-static analysis and correspondent experimental procedure.

3.1. Quasi-static Model

For the bumper structure, the quasi-static test that better matches the front crash situation with a full overlap is the compression of the structure between two rigid bodies in the direction correspondent to the velocity of the vehicle. If the behaviour of the structure is close to the numerical model in terms of deformation and energy absorption, the quasi-static model is validated and a similarity is expected between the dynamic crash model and a real crash.

For the computational simulations performed in this work, a generic process was used with the numerical tools available. Figure 1 sums the process in a flowchart.

In order to simplify the assembly of the structure for the experimental tests, as well as minimizing the manufacturing cost, the part sections were chosen from a catalogue of standard extrusion profiles. The geometry is represented in Figure 2 and was created using $CATIA^{TM}$ *V5*.

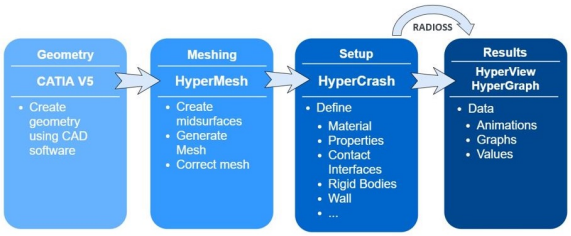

Figure 1: Flowchart of the process used to build the numerical model

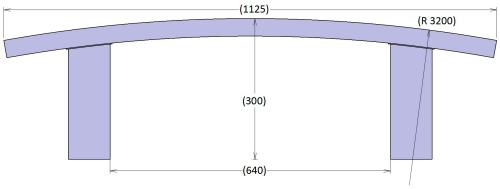

Figure 2: Bumper geometry measurements

The mesh was generated and improved using *HyperMesh®*. *HyperCrash™* was used to make the setup. The material model, contact interfaces, properties and boundary conditions were introduced at this phase. In order to mimic the experimental compression test, the structure must be compressed between two rigid structures. In this case, one of these structures is the rigid wall, placed at the front end of the bumper, and the other was defined with two rigid bodies, one on the end of each crash box. To these bodies a constant imposed velocity of 500 mm/s was defined.

After running the analysis using *RADIOSS™* explicit software, the data was treated using *HyperView®* and *HyperGraph®*. The summary of the crash performance of the modeled baseline structure described in this section is summarized in Table 2.

Table 2: Quasi-static model data

	Data	Value
F_{max}	Peak Crash Force [kN]	154.6
F_{avg}	Average Crash Force [kN]	87.9
EA	Energy Absorption [J]	19780
M	Mass [kg]	3.421
δ	Displacement [mm]	225
SEA	Specific Energy Absorption [J/kg]	5782
CFE	Crash Force Efficiency	0.57

3.2. Validation

Several extruded aluminum suppliers were contacted to obtain extruded aluminum profiles as close as possible to the ones chosen for the quasi-static model. At the time of this work, the chosen alloy was not available from any of the suppliers. The closest option in terms of properties and the one used for this validation procedures was the aluminum 6063 alloy with T6 heat treatment.

The material was tested according to the standard ASTM B557M-15 - Standard Test Method for Tension Testing (Metric) [8]. In order to have the best possible proximity to the material used in bumper structure analyses, the samples were cut from the same aluminum 6063-T6 extrusion tubes that will be used to build the complete structure. 15 samples were cut having the same axial direction, corresponding to the direction of the extrusion process.

After each of the samples is tested until fracture, a photo of the fractured sample is taken and the machine output was collected. The output consists of the stress-strain curve of each sample as well as values for axial and transverse elongation. From the curve, the values of elasticity modulus, yield strength, ultimate strength and elongation at break were obtained. Poisson's ratio was obtained from the axial and transverse elongation.

As explained in Section 2, the material model used in this work is the Johnson-Cook material model. The value A from equation (3) is the yield strength that was obtained from the tensile procedures. Values for Young's modulus (E), Poisson's ratio (ν), elongation at break (ε_{max}) and plasticity yield stress or yield strength (σ_{yield}) were collected, averaged and used as an input in the computational model. Comparing tabulated values [9] with the averaged values obtained in the tensile procedures, both E and ν are around 12% higher than expected, while the value for the yield strength has less than 1% difference. The largest difference occurs in the value of elongation at break that is 2.5 times lower than expected. This is an indicator that the material is a lot more brittle than expected. This comparison is listed in Table 3.

Table 3: Aluminum 6063 T6 properties

Property	Tabulated	Obtained
E [GPa]	68.9	61.69
ν	0.33	0.37
σ_{yield} [MPa]	214	215.68
ε_{max} [%]	15	6.17

A "fit" of the parameters B and n was made using Microsoft Excel solver funcionalities, minimizing the distance of each point to the average of the curves obtained from the tensile procedures. The optimum values for parameters B and n were obtained ($B = 0.0776$ and $n = 0.2115$). The resulting curve is shown in Figure 3.

The section of the tubes was also not possible to be the same of the one used in the quasi-static model. The measurements of the used geometry in the compression procedure are represented in Figure 4. The transverse beam could not be bent, so a straight beam was used.

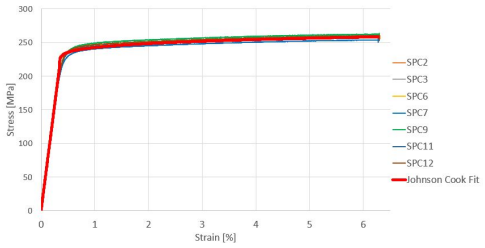

Figure 3: Johnson Cook material model curve compared with tensile test results

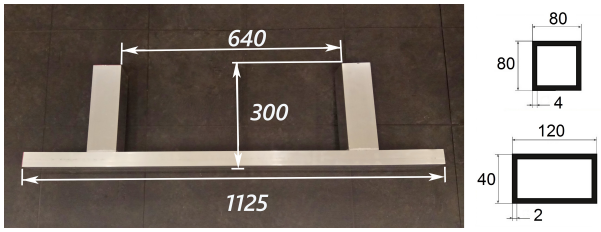

Figure 4: Compression procedure specimen measurements

The changes in material and geometry were introduced in the model. After running the analysis, the resulting force-displacement curve showed that this structure would go substantially above the force limit of the testing machine so the model was adapted to a compression of half of the structure. Three identical structures were compressed and the experimental force-displacement curves were collected and compared with the model data as shown in Figure 5.

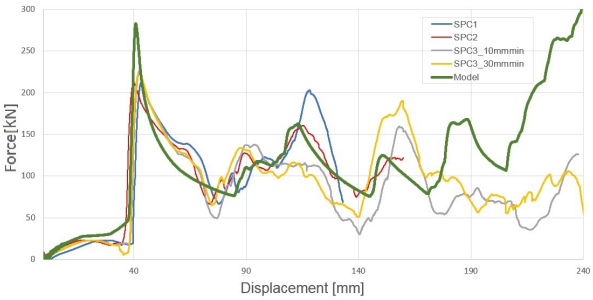

Figure 5: Experimental results vs quasi-static model

Extensive fracture was observed in all specimens. The fracture initiated in all the cases for a displacement value close to 75 mm. It is clear that, after that value, the curves do not have a good correlation. The expected deformation pattern was not observed in any of the specimens. This was expected since the material had lower ductility than required. Taking into account that the first fracture occurred at around 75 mm of displacement, it is clear that, after fracture, the curves do not have a good correlation. Nevertheless, the initial peak happens also at 40 mm of deformation and the force distribution before that is comparable, validating the model before the fracture. It would be expected that a material with the desired ductility would not break in this procedure and would have a closer correlation to the numerical model.

3.3. Dynamic conversion

With the main goal of this work in sight, the structure must be improved to perform as well as possible in a crash situation. The two most important motivations are the safety of the passengers and the performance in the crash test made by NCAP at 50 km/h onto a rigid wall. To make the structure meet a specific goal for a given vehicle project, it is important to take into account the mass of the vehicle and the vehicle speed at the moment of the crash. That way, the energy that the bumper structure is supposed to absorb in a specific front crash situation can be optimized. According to Campos et al. [10], the percentage of energy absorbed by the bumper deformable structure in a compact car is about 40%. In the present work, due to project requirements, the goal was an energy absorption of 50% of the crash energy by this structure for a vehicle of approximately 1400 kg, with the best possible performance.

Apart from the crashworthiness criteria, it is important that this EA process meets the requirements imposed by the regulations. These limits are imposed for a dummy full vehicle crash test. Due to the time line of this work, it was impossible to build a model for the whole vehicle and dummy, so some assumptions had to be made.

To convert the quasi-static model to a dynamic model, two important modifications needed to be made. The speed should be specified for the beginning of the test and mass should be added representing the vehicle. The initial velocity was specified to correspond to the frontal impact 50 km/h procedure made by NCAP into a rigid wall. To have the structure absorbing 50% of the kinetic energy of the vehicle, the mass added to the rigid bodies, representing the mass of the vehicle, is half of the expected vehicle's mass. The kinetic energy is directly proportional to the mass m and to the square of the velocity v,

$$E_k = \frac{1}{2}mv^2. \tag{4}$$

Inserting 350 kg on each of back ends of the crash boxes and performing the crash test is a decent approximation. In the end, the bumper should be able to absorb the kinetic energy and stop in a controlled and effective way, respecting the imposed requirements for a front crash test by NHTSA, described in Section 1.

Both quasi-static and dynamic test force-displacement curves were compared in terms of force distribution and deformation pattern to evaluate the comparability of both tests. In Figure 6 it is possible to see that the deformed structures were almost identical and both curves had a good correlation in all the crash and compression stages.

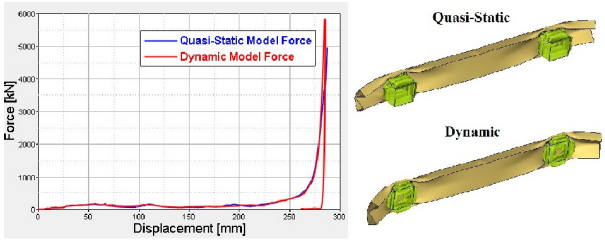

Figure 6: Comparison between quasi-static and dynamic tests

Both curves had a high peak of force at the end. In the quasi-static one, this peak happens because the structure was compressed over the maximum displacement. At that point of the test, all the structure could not deform any further, and the force grew exponentially. The same happened in the dynamic test but this growth in force stopped when all the kinetic energy was absorbed and the structure stoped. The two curves can be compared in detail before this growth in force starts in Figure 7.

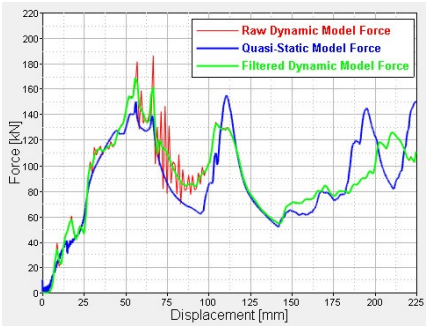

Figure 7: Comparison between quasi-static and CFC 1000 filtered dynamic test

It can be noted that both models are similar in terms of force displacement curves. However, when dimensioning the structure, all the curve should be considered because the structure should absorb enough energy for a specific range of deformation to avoid the force peak in the end of the curve in Figure 6.

For the considered mass and speed values, the value for the kinetic energy is $E_k = \frac{1}{2} \times 1400 \times 13.889^2 = 135033\ J$. The goal is to absorb 50% of this value with the bumper structure, so the baseline structure should absorb at least 67516 J. In Table 4 the values for the absorbed energy of the quasi-static and the dynamic models are compared with the kinetic energy of the full vehicle.

Table 4: Energy absorption of quasi-static and dynamic models

	Quasi-Static	**Dynamic**	**Kinetic Energy**
EA [J]	19780	20609	135033
$\%E_k$	15	15	100

These values show that the baseline structure cannot absorb enough kinetic energy of the considered impact test and thus must be optimized to meet the design requirements. The project goal is to get a structure that can absorb 50% of the kinetic energy without going above 60 G's of acceleration. The baseline structure can only absorb 15% before the maximum deformation is reached and the force grows exponentially.

4. Optimization

The optimization of the studied structure was made using the dynamic model. Using the dynamic model allows to mimic the real crash test and see of the structure is absorbing enough energy before reaching the maximum deformation. When all the kinetic energy is absorbed, the structure will stop. With this model, computation time can also be saved. The impact of a structure using this model lasts up to 100 ms. Remembering that the explicit integration uses time steps, the quasi-static model has a computational time at least five times higher because the compression lasts at least 500 ms.

4.1. Criteria of Crashworthiness

In order to assess the crashworthiness of the studied structure or compare the performance of different structures, it is necessary to establish proper criteria. The analyzed quantities must be relevant to the case study and previously proven useful in the comparison between crash structures. In several structural studies, a group of parameters have been used numerous times [11] and proven to satisfy these requirements. Some of these quantities will be used in the present work, namely the Energy Absorption (EA), the Specific Energy Absorption (SEA), the peak crash force (F_{max}), the average crash force (F_{avg}) and the Crash Force Efficiency (CFE).

The energy absorption of the structure during a crash can be obtained as $EA = \int_0^\delta F(z)dz$, where $F(z)$ is the crash force and δ is the deformation. The ratio between the absorbed energy and the mass m of the structure gives the SEA,

$$SEA = \frac{EA}{m}. \tag{5}$$

During the crash, the maximum force point gives the peak crash force, $F_{max} = max(F_z)$.

When the EA is obtained, it is possible to divide it by the total displacement, yielding the average crash force, $F_{avg} = \frac{EA}{\delta}$.

Dividing the average crash force by the peak crash force, results in the CFE,

$$CFE = \frac{F_{avg}}{F_{max}}. \quad (6)$$

If the average crash force is maximized and the maximum crash force is minimized, CFE is close to unity. The best possible scenario is when a structure absorbs energy with a value close to 1 for CFE.

4.2. Performance Evaluation

A Crashworthiness Score (CS) was used to compare the crashworthiness of each structure to the reference one, balancing the values of each of the crashworthiness criteria. Weights can be defined for each of the two criteria as w_1 and w_2, having $0 < w_1, w_2 < 1$ and $w_2 = 1 - w_1$. CS was given for a specific weighting (i) as

$$CS_i = w_1 \frac{SEA_i - SEA_{ref}}{SEA_{ref}} + w_2 \frac{CFE_i - CFE_{ref}}{CFE_{ref}} \quad (7)$$

In different scenarios with different requirements this weighting can vary but in the present work, Pareto analysis was used to evaluate the influence of each of the criteria and obtain the best design point considering a range of weightings in a multi-objective approach. This analysis was used in several structure iterations, changing several parameters in each of the iterations.

For each value of w_1 and w_2, one of the geometries have the highest CS and that is our optimum geometry for that weighting. All of the optimum geometries, corresponding to each of the weightings were located in a chart and, in the end, that is our Pareto chart that can be used to chose the best solution.

The points corresponding to the weightings of $w_1 = 1$ and $w_1 = 0$ represent the limits of the set, corresponding to the geometries with higher SEA and higher CFE respectively. A utopia point having the maximum SEA and CFE can be identified and the best compromise solution will be the one that is non-dimentionally closer to this point. This distance is evaluated by

$$d = \sqrt{\left(\frac{SEA_{max} - SEA_i}{SEA_{max} - SEA_{min}}\right)^2 + \left(\frac{CFE_{max} - CFE_i}{CFE_{max} - CFE_{min}}\right)^2}. \quad (8)$$

Regarding the regulations described in the beginning of this chapter, a limit acceleration of 60 G's will be imposed to the structure. At this point, if our optimal solution does not meet this requirement, the next point closer to the utopia point is the optimal solution.

4.3. First Iteration

The first iteration was made to the crash boxes as they are the component that absorb most of the energy in a frontal crash. Two parameters were chosen to be modified in the crash boxes to improve their EA ability and minimize as much as possible any force peak in the vehicle. The chosen parameters are represented in Figure 8. For this first iteration, the length L of the crash boxes and the wall thickness A of this section were modified and it is expected that an optimum solution is found.

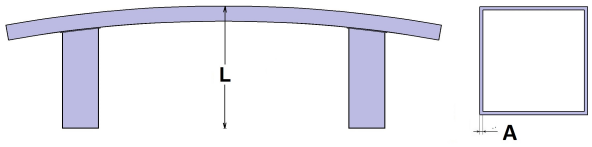

Figure 8: Parameters that were changed in the first iteration

Five values for A, between 2 mm and 4 mm, and four values for L, between 300 mm and 600 mm were tested. After analyzing the results using the performance evaluation described before with 101 different values for w_1 and w_2 (from 100% to 0% changing 1% in each), four optimum points were obtained as illustrated in Figure 9.

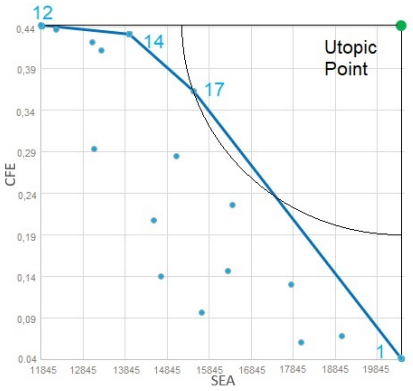

Figure 9: Pareto set of first iteration (each point corresponds to a different geometry)

Having the utopia optimum point at the right top corner of the Pareto set, the optimum geometry was chosen using equation (8). Also, the acceleration values must be considered in order to see of the chosen geometry satisfies the 60 G's criteria.

In Table 5 it can be seen that the optimum corresponds to geometry 17 but this geometry, as well as geometries 14 and 1, has a value for maximum acceleration higher than 60 G's. So the choice for the first iteration was geometry 12, with 3 mm thickness and 600 mm from the front to the back of the structure.

Table 5: First iteration geometry choice

Geometry	SEA [J/kg]	%Δ SEA	CFE	%Δ CFE	d	Max. acc. [G's]
12	11845	-42.0	0.443	+959.0	1	51.4
14	13935	-31.7	0.432	+924.4	0.76	72.4
17	15467	-24.2	0.363	+769.7	0.61	114.1
REF 1	20412	–	0.042	–	1	851.9

When comparing geometry 12 with the reference geometry, a major improvement can be verified. The peak acceleration dropped from 851 G's to 51 G's, meaning that the initial criteria for the maximum acceleration is satisfied. The mass of this structure is close to 67% higher, resulting in a 42% decrease in SEA but having a 959% increase in CFE. The higher value of CFE means a more evenly distribution of force over the crash. This can be seen in Figure 10 where the improvement can be noted. The peak at the end of the crash was avoided because the structure was able to absorb all the energy before the maximum deformation value.

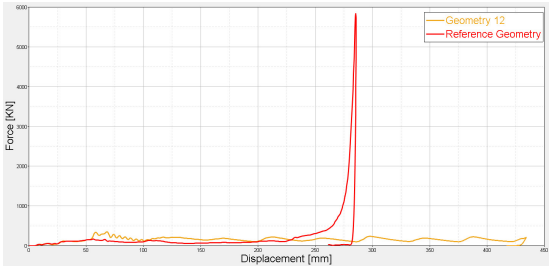

Figure 10: Comparison between the reference geometry and geometry 12 force-displacement curves

4.4. Second Iteration

In the second iteration, the beam must be reinforced to obtain a better distribution of force in the beginning of the crash. Two reinforcement options were studied: the increase in thickness of the beam and the use of an internal rib that divides the interior of the beam, creating two closed cells. Also, in the first 20 mm of deformation, the force is specially low because this corresponds to the period when the curve transverse beam fits to the wall before starting to crush. Taking this into account, two more values of curvature were also tested to have a better understanding of the influence of this parameter in the energy absorption performance.

The three parameters of this iteration are represented in Figure 11. Four values between 2.5 mm an 4 mm were tested for the thickness. In terms of curvature, 3200 mm and 2000 mm values for the radius were compared with a straight beam.

The same process used for the first iteration was repeated. Table 6 contains the results correspondent to the four geometries in the Pareto set, compared with the reference.

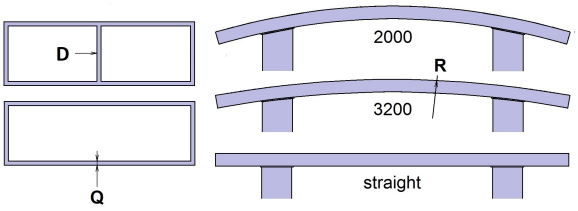

Figure 11: Parameters that were changed in the second iteration

Table 6: Second iteration geometry choice

Geometry	SEA [J/kg]	%Δ SEA	CFE	%Δ CFE	d	Max. acc. [G's]
12	9735	-17.8	0.562	+26.9	1	43.7
18	10508	-11.3	0.560	+26.5	0.66	43.0
21	11633	-1.8	0.536	+21.0	0.26	44.2
9	12007	+1.4	0.440	-1.9	1	51.3
REF 5	11845	–	0.443	–	–	51.4

The geometry with internal rib, R = 2000 mm and Q = 2.5 mm (Geometry 21) had the closest point to the utopic point. Comparing the crashworthiness criteria of the geometry obtained in the first iteration (REF 5) with the new optimized solution, a 21% increase of CFE was verified with less than 2% decrease in SEA. The curvature was increased from a radius value of 3200 mm to 2000 mm. Both structures have the same wall thickness and the new structure weights 200 g more due to therib. Comparing the energy absorption of both structures in the first 50 mm of deformation, the reference geometry absorbed 3350 J while the new optimized geometry managed to absorb 4332 J. Although, the values of absorbed energy in this section are low when compared to the energy absorption in the rest of the crash. The first 50 mm of deformation still have a low force distribution but the overall efficiency was improved. The force peaks have been decreased and the average force increased. The new structure have a maximum peak that corresponds to 44 G's.

4.5. Third Iteration

After two iterations to the geometry, the performance has been improved substantially. The improvement was mostly due to the improvement of CFE by lowering the peak force and growing the average force. At the start of the crash boxes deformation, still exists a higher force peak. In the third iteration, different sections were tested for the crash boxes. The goal was to lower the initial peak or increase the overall force distribution to make it more uniform and, if possible, save weight without compromising the performance.

Two more parameters were studied to see their influence in the initial buckling of the structure as well as in the folding pattern, shape and width of the crash boxes. In Figure 12, the shapes used in this iteration are represented.

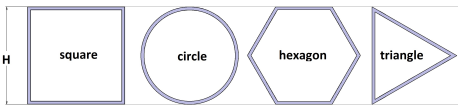

Figure 12: Parameters that were changed in the third iteration

The same process used in the first and second iterations was followed. Table 7 contains the data corresponding to the SEA, CFE, maximum acceleration and non-dimensional distance to the utopic point of each of the three geometries in the Pareto set, compared with the reference.

Table 7: Third iteration geometry choice

Geometry	SEA [J/kg]	%Δ SEA	CFE	%Δ CFE	d	Max. acc. [G's]
8	13008	+11.8	0.729	+36.1	1	40.6
6	13852	+19.1	0.703	+31.3	0.37	39.8
16	14339	+23.3	0.385	-28.1	1	54.8
REF 3	11633	–	0.536	–	–	44.2

The geometry with circular section and 85 mm (Geometry 6) width was the choice after this iteration, having the lowest non-dimensional distance to the utopic point. The circular crash boxes had, by far, the best uniformity in force through the crash. It can also be concluded that this uniformity is related with the number of faces. The geometries with more faces had a better force distribution and that makes sense since, by increasing the number of faces it gets closer to a circle.

4.6. Fourth Iteration

At this point, the value of CFE reached 0.7 that is a satisfactory value for this parameter. The next approach had weight decrease as main goal, trying to make the structure as light as possible, without affecting the value of CFE significantly. If the weight is decreased, it is expected that the performance is higher having an increase in SEA.

As mentioned before, the transverse beam absorbs a negligible amount of energy on a front crash when compared to the crash boxes. In particular, for the optimal geometry of the previous iteration, the energy absorbed by the transverse beam was 12% of the total energy.

Having that in mind, the section of the beam were be changed to reduce weight. The tested structures had reduced widths as well as a smaller size for the front and rear surfaces. In Figure 13 the reference section for this iteration is at the left and the changed measurements at the right. The width Z was varied between 20 mm and 60 mm, B between 100 mm and 120 mm and I between 60 mm and 120 mm. Table 8 contains the results correspondent to the three geometries in the Pareto set.

Table 8: Fourth iteration geometry choice

Geometry	SEA [J/kg]	%Δ SEA	CFE	%Δ CFE	d	Max. acc. [G's]
REF 10	13852	–	0.703	–	1	39.8
8	16642	+20.1	0.649	-7.8	0.57	41.7
9	17249	+24.5	0.602	-14.3	1	44.8

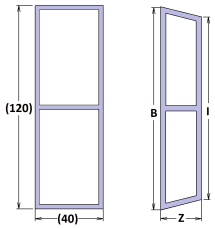

Figure 13: Parameters that were changed in the fourth iteration

Following the same criteria of the previous iterations, the geometry with Z = 20 mm, B = 100 mm and I = 90 mm (Geometry 8) was the choice after this iteration, having the lowest non-dimensional distance to the utopic point. The force distribution was not substantially affected but the weight of the structure was reduced in 1 kg that represents 20%. This translated into a 20% increase in SEA with less than 8% decrease in CFE.

4.7. Final Results

At the end of the fourth iteration, as expected, the final structure had a better performance in general, when compared with the initial reference. The comparison between the two, in terms of measurements, as well as the sum of the improvement made to the structure after the four iterations is shown in Table 9. Figure 14 shows the difference in shape and deformation pattern of the initial and final structures.

Table 9: Initial vs final geometries comparisson

Geometry	A [mm]	L [mm]	D [yes/no]	R [mm]	Q [mm]	Shape	H [mm]	Z [mm]	B [mm]	I [mm]
Initial	2	300	no	3200	2.5	square	95	40	120	120
Final	3	600	yes	2000	2.5	circle	85	20	100	90

Geometry	SEA [J/kg]	%Δ SEA	CFE	%Δ CFE	Max. acc. [G's]	%Δ Max. acc.	Mass [kg]	%Δ Mass
Initial	20412	–	0.042	–	851.9	–	3.421	–
Final	16642	-18.5	0.649	+1451.8	41.7	-95.1	4.088	+19.5

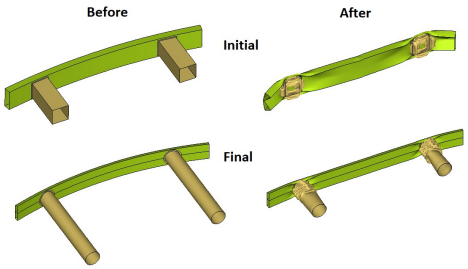

Figure 14: Comparison between the initial geometry and the resultant of the optimization process

The final structure had close to 20% more mass than the initial one, translating into a 19% decrease in SEA. The final structure is able to absorb energy with a force curve always below the maximum established value of 60 G's and the CFE parameter increased more than 14 times, meaning that the force

displacement curve is much more uniform than the initial one.

Compiling all the tested geometries in the four iterations in Figure 15, the progress of each iteration in terms of crashworthiness criteria is clear.

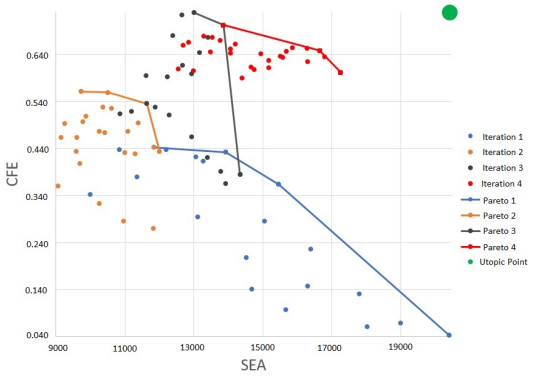

Figure 15: Final Pareto distribution

5. Conclusions

After all the iterations, testing of a significant number of alternatives and studying the parameters influence in the crash performance of the frontal impact energy absorption system, a robust numerical model was built. The material model used has a good correlation with previous works regarding thin-walled beams axial compression, although it could not completely validated in this work, due to lack of quality of the provided material by the suppliers at hand.

A versatile and adaptable multi-objective evaluation methodology was developed and proven to have good results by improving the structure, regarding the used crashworthiness criteria.

A robust explicit non-linear numerical model was built, suitable for dynamic or quasi-static setups, using simple structures, composed by one ore more thin-walled beams with changeable shape and material. A solid and goal-oriented multi-objective optimization procedure was achieved, that can be adapted to fit future goals of the project or any multi-objective project. The collected data and the evaluation system allows the gathering of information about the influence of each of the tested parameters in the crash performance. The final optimized structure meets the initial goals in terms of deceleration of the vehicle in the occurrence of a frontal impact similar to NCAP 50 km/h solid barrier front crash procedure. For a traditional bumper composed of a transverse beam and two crash boxes, the beam was proven to have low influence in terms of energy absorption during front collision. The curvature of the transverse beam was proven to be beneficial, initiating the crash box deformation for a lower value of force. The use of crash boxes of circular section was the best improvement in the optimization, providing a way to save weight, while improving the force-displacement curve.

References

[1] World Health Organization. Global status report on road safety 2015.

[2] William T. Hollowell, H. C. Gabler, S. L. Stucki, S. Summers, and J. R. Hachney. Updated review of potential test procedures for FMVSS no.208, 1999.

[3] European Aluminum Association. Applications - car body - crash management systems. *The Aluminum Automotive Manual*, 2013.

[4] Gordon R. Johnson and William H. Cook. Fracture characteristics of three metals subjected to various strains, strain rates, temperatures and pressures. *Engineering Fracture Mechanics*, 21(1):31–48, 1985.

[5] Len Schwer. Optional strain-rate forms for the Johnson Cook constitutive model and the role of the parameter epsilon_01. *6th European LS-DYNA Users Conference*, 2007.

[6] Office of Aviation Research. Failure Modeling of Titanium 6Al-4V and Aluminum 2024-T3 With the Johnson-Cook Material Model. *U.S. Department of Transportation - Federal Aviation Administration*, Sep 2003.

[7] A. Manes, L. Peroni, M. Scapin, and M. Giglio. Analysis of strain rate behavior of an al 6061 t6 alloy. *Procedia Engineering*, 10:208–2183477–3482, 2011.

[8] ASTM B557M-15. Standard test methods for tension testing wrought and cast aluminum- and magnesium-alloy products (metric). *ASTM International*, 2015.

[9] Aerospace Specification Metals Inc. Aluminum 6063-T6. `asm.matweb.com`. Accessed July 2017.

[10] José Ángel Lṕez Campos, Abraham Segade Robleda, José Antonio Vilán Vilán, Paulino José García Nieto, and Javier Blanco Cordero. Study of a steel's energy absorption system for heavy quadricycles and nonlinear explicit dynamic analysis of its behavior under impact by fem. *materials*, Oct 2015.

[11] T. Tang, W. Zhang, H. Yin, and H. Wang. Crushing analysis of thin-walled beams with various section geometries under lateral impact. *Thin-Walled Structures*, Jan 2016.